LAWRENCE
LIVERMORE
NATIONAL
LABORATORY

LLNL-JRNL-613413

Observations on shock induced chemistry of cyclohexane

M. C. Akin, R. Chau

January 28, 2013

Journal of Chemical Physics

Disclaimer

Observations on shock induced chemistry of cyclohexane

M. C. Akin* and R. Chau

Lawrence Livermore National Laboratory,

University of California, Livermore, CA 94550

(Dated: April 8, 2013)

Abstract

We use double pass absorption spectroscopy to examine shock induced reactions *in situ* in cyclohexane and benzene at pressures up to 33.1 GPa. Reactions in cyclohexane begin by 27 GPa and complete by 33.1 GPa. Reactions in benzene are observed to begin by 12 GPa and are complete by 18 GPa. Absorption spectra indicate that the first reaction in cyclohexane occurs within or near the shock front, and that a metastable local equilibrium is reached in the post-shock state. A second process may be observed upon reshock at the lower pressures, suggesting a new equilibrium is reached post-reshock as well. Absorption bands are consistent with the formation of short radicals or fragments upon decomposition; however, spectral resolution is too low to confirm this mechanism.

PACS numbers: 62.50.-p, 82.40.FP, 82.20.-w, 82.40.-g,82.30.LP

*Electronic address: akin1@llnl.gov.

I. INTRODUCTION

New applications and materials demand a better understanding of chemistry at extremely high pressures (P), temperatures (T), and densities (V). High pressure platforms, planetary models, and high explosives have led to increased interest in understanding shock initiation of reactions, shock heating, and how extreme conditions affect materials. A broad model that connects benchtop chemistry with chemistry at extremes would allow existing detailed chemical models to be leveraged to understand extreme chemistry. The difficulty of executing chemical studies under these conditions hinders the development of such a model. Static studies in diamond anvil cells have upper limits on the pressures and temperatures available; to achieve the highest pressures, a system must be dynamically compressed. Time, volume, and length scales in these studies are short, making data collection a challenge. *In situ* probes of bonding and mechanisms are likely to be affected by high background levels and pressure and thermal effects. Shock-driven reaction conditions vary widely, leading to many possible products, some of which may surprise an"ambient" chemist and complicate post-shock or recovery analyses. Recovery analyses are further complicated by possible reactions occurring upon decompression. As a result of these difficulties, most research so far has studied the macroscopic P, T reaction conditions, and has used a sharp change in density with pressure (a "cusp" in the Hugoniot) to identify the existence of a reaction. Less work

has been done on identifying the reaction details essential for connecting shock chemistry to ambient chemistry.

The contrasts between benzene and cyclohexane highlight the role of bonding, especially aromatic bonds, in shock chemistry. Benzene (C_6H_6) and cyclohexane (C_6H_{12}) are classic models of hydrocarbon bonding and stability, with benzene representing thermally stable aromatics, and cyclohexane the thermally unstable hydrogenated ring. These materials behave very differently under shock compression: benzene shows an obvious reaction cusp at ∼10 GPa, while cyclohexane does not show a similar cusp at pressures up to ∼43 GPa.[1]

Due to its importance in explosives chemistry, benzene has been studied more at high pressures and under shock conditions than cyclohexane. In thermally driven, low pressure reactions typical of benchtop chemistry, benzene is much less reactive than cyclohexane. Under cold, high pressure environments (e.g., diamond anvil cells), benzene is also stable; 30 GPa is required at room temperature to drive the irreversible chemical reactions of benzene,[2] with no reactions observed below ∼20-23 GPa. [2, 3] Under the higher temperature environment of a shock, different products are recovered [3] and reactions occur at much lower pressures, around 10 GPa. [1].

Cyclohexane, though not common in high explosives, is an excellent simple model for hydrogenated species such as plastics and hydrocarbons, which are increasingly used in high pressure physics. To illuminate these effects in shock driven reactions, cyclohexane must be studied and compared to benzene at pressures where cyclohexane reacts. Existing work studying cyclohexane in shocks and diamond anvil cells have shown it to be stable up to ∼20 GPa.[1, 4–12, 14**?** –17]

A comparison of Dick's Hugoniot[1] for cyclohexane to the Universal Liquid Hugoniot shows small deviations occurring around 22-24 GPa, [18, 19] suggesting a reaction or other phase change may begin in that region. A recovery experiment by Barabe *et al.* [17] showed that cyclohexane shocked to 43 GPa produces traces of hexene, but the product levels are less than 1% of that observed in benzene for a similar shock. The chemistry of cyclohexane above 22 GPa has not been studied *in situ*. Reaction mechanisms, timing, and P,T conditions, as well as intermediate products, are unknown.

To explore the reaction mechanisms of cyclohexane and shed light on the different shock responses of aromatic and hydrogenated rings, we perform a series of shock wave experiments using double pass absorption spectroscopy to study the *in situ* chemistry of cyclohexane for

the first time. We demonstrate that a strong shock wave induces reactions in cyclohexane near the predicted pressure, with a focus on the time and length scales of this process. Based on the absorption spectra, we can constrain the reaction types, initiation times, and intermediate products. Our experimental design also includes the effects of a reshock to attain higher pressures, and the resulting effects on absorption and scattering that are more generally applicable to materials at extreme conditions.

II. EXPERIMENT

The targets used for these experiments comprise an aluminum (Al1100) target body with a 3 mm thick diamond turned aluminum (Al1100) baseplate containing a cavity, and a 3 mm thick quartz window, as shown in Figure 1. The diamond turned baseplate provides a mirror finished surface for the double pass optical spectroscopy. Ports in the Al target body allow the 5 mm thick sample cavity to be filled with benzene or cyclohexane. The targets are filled using a vacuum flow system that circulates the fluid through the sample cavity to prevent air bubble formation. The thick sample provides a long time for the shock wave to travel through the sample and the experiment is over before the shock wave breaks out of the quartz window.

For the reader unfamiliar with shock physics, we will give a brief outline of the shock processes in this experiment. For a thorough explanation, the interested reader should consult Zel'dovich and Raiser. [20] A two stage light gas gun launches an Al impactor toward the target baseplate. In this study, the impactor velocities range between 3.6 and 6.4 km/s. Impactor velocities are measured by flash x-ray photography and have $< 0.1\%$ uncertainty. The impact of the flyer launches a shock wave in the Al baseplate. The shock front is narrow and moves through the material at the shock speed, U_s. Before the shock, a material has an initial density ρ_0 or V_0 ($\mathrm{V}_0 = \rho_0^{-1}$), temperature T_0, and particle speed $U_{p,0}$ (which is zero, as the sample is not moving). As the shock passes, it imparts energy to the material, resulting in higher local particle velocity U_p. It also compresses and heats the material to a local P and T. The shocked P, T, and U_p depend on the strength of the shock, which is determined by the impactor velocity. The collection of shock states available from a specific starting point in P, V, T space is known as the shock Hugoniot. As the shock passes from one medium to another, e.g., Al to cyclohexane, conservation laws require that P and

U_p at the interface be constant. Cyclohexane is less dense than aluminum, so P decreases and U_p increases when the shock enters the cyclohexane; as a result the aluminum is said to release. This local released U_p is the speed of the Al/cyclohexane interface that serves as the mirror, and is determined by the intersection (impedance match) of the cyclohexane Hugoniot and the Al release path in P-U_p space. When the shock arrives at the denser quartz window, U_p at the cyclohexane/quartz interface drops and P increases, launching a shock into the quartz and a *reshock* back into the cyclohexane. The Hugoniots, releases, and their associated U_p-U_s relationships used in this study are experimentally determined, while the reshock Hugoniot of cyclohexane is approximated.

Previous benzene experiments at 12 and 18 GPa are repeated. The cyclohexane experiments are performed between 27 and 33.1 GPa. At these pressures, the shock wave takes $\sim$ 500-600 ns to transit the organic sample. Shock velocities and pressures in Al are calculated by impedance match to the flyer velocity using data from Mitchell and Nellis [21]. To calculate the shock pressure in cyclohexane, a reflected Hugoniot is used to approximate the released Al U_p, which contributes $\sim$1% uncertainty. This particle velocity is impedance matched to Dick's Hugoniot, [1] where the shock speed is

$$U_s = 1.675 + 1.645U_p - 0.023U_p^2. \tag{1}$$

Pressures calculated from this method have a total uncertainty of $\sim$3%. Reshocks in cyclohexane are calculated using a reflected Hugoniot and impedance matching to quartz. These reshock pressures are well above the Hugoniot elastic limit in quartz, even in the lowest pressure shots. The top pressure in the cyclohexane Hugoniot studied by Dick [1] was 43 GPa; all of the reshock pressures are above this value, so we can only estimate the uncertainties in reshock pressure. The lack of data in this region combined with uncertainties in the quartz Hugoniot lead us to estimate the uncertainty in reshock as double the uncertainty in shock, or 6%. However, we note that since we do not have direct measurements of the quartz velocity, it is possible that the reshock pressures may have larger uncertainties.

The absorption spectroscopy is based on the methods of Kormer [22] and Holmes. [23] The optical system consists of a custom made fiber optic bundle of seven 400-μm diameter silica fibers mounted against the quartz window of the target (see Figure 1). The probe light is generated by a flash lamp powered by a pulse-shaped capacitor-discharge unit providing

a 60 μs square pulse. The duration of the experiment is $\sim 1\mu$s, and the pulse during this time is flat. The light from the source is focused into the center fiber of the bundle using a microscope objective lens. The light exits the fiber bundle, passes through the sample, reflects off the diamond turned Al baseplate and is collected by the six fibers surrounding the center fiber. The light from each of the six fibers is fed into a narrow band pass filter, a set of neutral density (ND) filters, and finally a photomultiplier tube. For these cyclohexane experiments, the narrow band pass filters are chosen to cover 400-650 nm in 50 nm increments. The benzene experiments used 532 nm light from a laser source. Prior to each experiment, each fiber bundle is calibrated against a known spectral source. The ND filters for each shot are chosen to give signals within the linear response region of the photomultiplier tubes based on the calibration of the fiber bundle and the expected radiance for that pressure. Signal from the PMT output is measured by oscilloscopes every 2 ns at 27 and 34 GPa, and every 400 ps at the other pressures. The response time of the PMTs is faster than the sampling rate in both cases and does not impact the data. No velocimetry measurements were made on these shots, so a multiple-wave structure, if present, is not detectable.

III. ANALYSIS

A. Correction for geometric changes in collection efficiency

In this geometry, the light captured increases as the baseplate gets closer to the fiber bundle. Thus for a completely transparent material the light level will increase as a function of time once the shock wave enters the sample. This effect is corrected using a mathematical prescription to determine the effective scattering, described in detail by Holmes.[23] This effective scattering is based on the initial distance of the fiber bundle to baseplate ($h = 8$ mm); numerical aperture ($\alpha = 0.22$), spacing ($R = 330\mu$m), and radius ($r_f = 200\mu$m) of the bundled fibers; the refractive index of the shocked and unshocked sample (n' and n, respectively); and a roughening factor (a). As cyclohexane's refractive index under shock conditions is not measured in this experiment, we calculate it using the Gladstone-Dale equation,

$$n' = 1 + (n-1)/(1 - U_p/U_s), \tag{2}$$

which has been found to be consistent with observed values. [14] The roughening factor accounts for decreases in baseplate reflectance once the shock passes due to roughening at the baseplate/sample interface. Holmes [23] determined that the correction factor for roughening is required in shocked samples, which is determined and applied for each channel in our study. While we use the full derivation in correcting the geometry, space limitations preclude reproducing it here. Our geometry is identical and thus no alterations to the derivation are required. The most important resulting equation is that of the effective scattering, which takes the form of

$$\eta_{eff}(a,t) = \begin{cases} \eta_{refl}(t) & \text{t} \leq 0 \\ a\eta_{refl}(t) + (1-a)\eta_{scat}(t) & \text{t} > 0, \end{cases} \tag{3}$$

where a is the "step size" that indicates proportional changes in reflectivity due to surface roughening (Fig. 2, inset). A step size of 1 indicates no loss in original reflectivity, a step of 0 indicates full loss. Step heights, determined by a fitting algorithm, are unitless. This fitting determines the signal for a non-reactive sample, and thus the geometric effects. This method requires that a null/fully absorbed PMT signal has zero voltage, which is set on the oscilloscopes prior to the experiment. Any DC signal observed prior to shock breakout is due to the original geometry and total light reflected through the organic sample prior to the shock, with step size due to changes in reflectivity scaling proportionally to the original signal. The constant DC signal observed prior to shock breakout indicates the lamp pulse is steady, with no color or luminance change during the experiment (that is, total brightness is constant during the experiment). Because each color band is scaled as a fraction of the pre-shock signal, spectral characteristics of the lamp (e.g., color temperature) or sensitivity of a specific PMT are self-corrected, and a separate reference for the lamp is not required. The geometric effects are subtracted from the observed absorption. The time dependent curve was then converted to distance using the shock speed, yielding the curves shown.

Changes in the calculated shocked refractive index do not affect the apparent step size, but only changes the curvature of the correction, with greater curvature occurring with increased refractive index. The difference in curvature is greater at longer times, but within the experimental time scale is minimal. For example, a 10% increase in the shocked refractive index leads to a 6% increase in the correction needed, even at late times (800 ns after

breakout); in the first 200 ns the correction for the relative change in refractive index is less than 1%. As a result, even if our calculation of the shocked refractive index is wildly inaccurate, leading to incorrect calculations of absolute absorbance, the relative changes in time, distance, and wavelength will remain very similar to those calculated in this paper.

Refractive index corrections for the quartz window were calculated using a refractive index value of 1.55. These corrections are not included in this paper because they are constant during the first shock and only affect the data after reshock. Including the effects of the quartz corrections after reshock artificially created discontinuities in the data which obscured important features near the reshock point. Instead, the data are shown without the window corrections, so that the near-reshock features, including the continuous absorption, are more easily seen. We will discuss here the interactions occurring during reshock which can affect the reshock data collection and interpretation.

Reshock pressures in this study range from ∼45-60 GPa, and in all cases the quartz will convert to stishovite,[24] which has a refractive index at ambient of ∼1.8. We used the Gladstone-Dale relations above to calculate the refractive index under compression in the quartz, which ranges between 1.9 and 1.95 in this study. This refractive index is comparable to what we calculate for both the shocked and reshocked cyclohexane, so transmission between shocked cyclohexane, reshocked cyclohexane, and shocked quartz is ∼1. Reflections occur between the shocked quartz and the unshocked quartz, which lead to a total reflection-based loss of the input light of ∼5% (at incident angles up to 30deg) according to Fresnel's equations. Thus we do not need to be concerned about the creation of a highly-reflecting surface in the window or at the sample-window interface due solely to changes in density and refractive index.

However, refractive index is not the only change to happen to quartz upon shock compression. As the quartz converts to the different crystal structure of stishovite, we assume that the single-crystal structure of the quartz is lost, to be replaced by multiple microcrystals of random orientation. These crystals, and defects associated with them, may serve as scattering centers, diffusing the light and increasing the apparent absorption. We expect this absorption change to increase linearly with time as the shock transits the quartz. Stishovite is clear to white, so we do not expect any wavelength-dependence to be seen in the scattering or absorption. Quantifying the absorption that results from reshock-driven reactions and that from microcrystal-induced scattering is not possible from these data. We

can state that stishovite does not become fully scattering; if that were to happen, absorption would rapidly jump to 1 following reshock. This was not observed to occur on any shot. As a result of the likely microcrystal formation, absorption following reshock should be regarded with some skepticism, and as qualitative rather than quantitative. In the best case scenario, wavelength-dependent differences in absorption slope *may* indicate changes in the absorption spectrum upon reshock.

B. Beer's Law, as applied in a changing cell volume

Absorption is typically treated as Beer's law under conditions where the cell size l is fixed ($dl/dt = 0$) and either the cross section $\epsilon[t, \lambda]$ or the concentration $C[t]$ of the absorbing species changes. Under shock conditions, the cell size is not fixed, but is determined by the shock wave speed: $dl/dt = U_s$. Beer's Law is

$$A[t, \lambda] = C[t]\epsilon[t, \lambda]l[t] \tag{4}$$

where l is the cell length; in this case, $l[t] = U_s t$. For simplification while considering the role of a changing absorption cell volume at a fixed wavelength, we will treat $C[t]\epsilon[t, \lambda]$ as a single function, $B[t]$. Other aspects and assumptions of Beer's Law, such as the requirement that the sample remains sufficiently dilute to avoid nonlinear response in absorption, must also be considered. We assume that cyclohexane remains non-absorbing in the visible, and that absorption is due to intermediates or products of the shock reaction, and that most intermediates proceed to recoverable products. Recovery experiments by Barabe indicate that the concentration of such products in cyclohexane at pressures up to 43 GPa are <1-2% level,[17] so the solution is dilute and Beer's Law applies.

We assume in this section that the nonlinear detector response can be neglected. There are then three possible responses that can appear in the absorption data:

1. $dB/dt = 0$. Under this arrangement, we find

$$\frac{dA}{dt} = B\frac{dl}{dt} = BU_s. \tag{5}$$

As a result, A increases at a constant slope BU_s with respect to time and position.

The requirement that B in the shocked region remains constant implies that a steady state is reached within experimental resolution of the shock front, or that the reaction is driven to completion within experimental resolution of the front. If the reaction continued beyond the shock front, dB/dt would be non-zero.[25] Since the absorbant concentration is set by the first shock transit and is also constant under these conditions, an estimate of $\epsilon[t, \lambda]$ can be made. Any change in the *slope* of the absorption is an indicator of a change in either $\epsilon[t, \lambda]$ or $C[t]$, though determining which function changes requires an independent measurement. Such a constant slope is shown in Figure 3.

2. $dB/dt > 0$. This occurs if reactions continue. For example, the shock front generates a large number of initial reactants, which are consumed to yield absorbing products. As the reactions progress in time, $B[t]$ within a given volume increases. This result can also be seen if $\epsilon[t]$ increases with time; for example, if significant broadening or intensification of an absorption band occurs, even if the absorbant concentration is constant. In these cases, A[t] is super-linear with respect to time.

3. $dB/dt < 0$. The shock front generates a large number of initial absorbing reactants, which are consumed in the post-shock region. As the reactions progress in time, $B[t]$ decreases, e.g., as absorbants are consumed or from a decreasing absorption cross section. In this case, A[t] is sub-linear with respect to time.

C. Estimating absorption spectra

To examine the effect of a stronger shock on the absorption spectra, and allow comparisons across pressure, the absorption spectra are normalized to the same transited mass of cyclohexane using the shock speed. Based on the data of Dick[1], absorption spectra, initially collected as a function of time, are mapped to physical dimensions using

$$x[t] = U_s t \tag{6}$$

Each channel is fit to a line in the form

$$B[t] = mx + b \tag{7}$$

Comparing m with regard to pressure highlights the changes in absorption, including those associated with the overdriven reaction.

IV. RESULTS

TABLE I: Calculated shock and reshock pressures for each shot. All impactors were Al 1100. Uncertainties in U_p are estimated to be 1% due to reflection of the Al Hugoniot used in impedance matching. Reshock pressures were calculated by reflecting the appropriate sample Hugoniot and impedance matching to the quartz Hugoniot. Due to the total absorption observed in benzene, we did not bother to calculate the reshock pressure. In the case of cyclohexane, no data exist for the Hugoniot above 43 GPa, so we have assumed the relative uncertainty of the reshock to be double that of the initial shock.

Shot	U_{flyer} km/s	Target	U_p km/s	U_s km/s	P GPa	Reshock P GPa
3957	5.613 ± 0.007	cyclohexane	4.23 ± 0.04	8.2 ± 0.3	27. ± 0.6	47 ± 3
3958	6.367 ± 0.007	cyclohexane	4.75 ± 0.05	9.0 ± 0.4	33.1 ± 0.7	57 ± 3
3982	6.135 ± 0.007	cyclohexane	4.59 ± 0.05	8.7 ± 0.4	31.1 ± 0.7	54 ± 3
3981	5.818 ± 0.006	cyclohexane	4.38 ± 0.04	8.4 ± 0.3	28.6 ± 0.7	50 ± 3
3854	3.623 ± 0.004	benzene	2.80 ± 0.05	5.93 ± 0.05	12 ± 0.2	n/a
3853	3.905 ± 0.005	benzene	3.01 ± 0.05	6.03 ± 0.05	17.7 ± 0.2	n/a

A. Roughening

Careful inspection of the data shown in Figure 3a reveals multiple processes. At x = 0 mm, the shock arrives, and over a few μm scale the absorption increases. In an unreactive medium such as water, the step size at breakout, a in Eqn. 3, is due to baseplate roughening and increased scattering. In the case of water, the step is ∼0.9, indicating a 10% loss of transmitted light; this roughening is not wavelength dependent. An experiment using overdriven benzene and looking at a single wavelength (532 nm) suggests that surface variation within a single shot is about 5%. These two results tell us that the step size can be expected to change by up to ∼ 15% due to physical roughening and shot-to-shot varation in scattering; any additional changes must be due to other processes, such as reactions.

Typical step sizes for cyclohexane are ∼ 0.7-0.85 (Figure 2). After accounting for surface roughening, the lower step height suggests an additional 5-20% decrease in transmission

at breakout compared to water, indicating the formation of scattering and absorption centers through reactive processes. At the highest pressures, these changes are observed at the sub-ns level. At the lower pressures these changes are most clearly observed at the shortest wavelengths. Step heights from the cyclohexane data also vary more across wavelengths than expected for a non-reactive medium, between 14% and 60% on a single shot, compared to the 5% that might be expected due to surface variation. Slight wavelength dependence is seen at lower pressures, but at the highest pressure there appears to be a strong wavelength dependence. At this pressure, the roughening factors at 600 and 650 nm are calculated to be slightly greater than 1 and rounded down; this is consistent with an increase in collected light, as would be expected if the sample began emitting (either via fluorescence or thermally) at these wavelengths. In contrast, short wavelengths on this shot show very strong decreases in collected light, consistent with strong absorbers/scatterers or a strongly wavelength-dependent refractive index. Water shots show that scattering from the baseplate is not strongly wavelength dependent, so this variation must be due to other causes arising from the chemical sample. Reactions resulting in immediate changes in ϵ, for example, through the formation of an excited free radical, are one obvious origin of such absorption changes. Another possible source is the formation of larger carbon-rich clusters which scatter through Mie processes. Both of these processes can show wavelength dependence corresponding to increased absorption at shorter molecular length. The different reactivities of different materials would also explain why different materials have such different roughening step sizes. The appearance upon breakout indicates that the reactions leading to scatterer formation occur rapidly, within the first 90-100μm, and likely within the shock front.

B. Absorption in cyclohexane

The data for each cyclohexane channel are shown in Figure 3 in increasing pressures between 27±0.6 GPa and 33.1±0.7 GPa. The data are plotted as the fraction of absorption (where absorption = 1 - transmission, including scattering effects) as a function of shock front position. Each graph's left half displays the absorption as a function of the front's position on the first transit; the right half displays the position of the reflected reshock front as it travels back toward the Al baseplate, as distance from the baseplate. This mapping

allows a direct comparison of absorption as a function of mass transited by the shock or reshock. The behavior of cyclohexane is strongly pressure and temperature dependent. Following the rapid rise in absorption due to surface roughening that marks shock breakout, slower processes dominate, presumably chemical and kinetic in nature.

At the lowest pressure, 27 GPa, the absorption increases linearly with mass transited by the shock (See Figure 3a). This constant slope is consistent with a reaction that goes to equilibrium within the shock front, as discussed in section IIIB. An incubation period of $\sim$ 40 ns may be present in the 27 GPa data (see inset, Fig. 3a). Such an incubation period is not observed on other channels or at other pressures, and this signal is present at similar to the noise level. During the first shock, absorption at 400 nm is roughly double that at 450-600 nm, where absorption is only weakly wavelength dependent. Beginning at 1.5 mm, some wavelength dependence appears as the absorption rate decreases at 650 nm. The onset of this decreased slope region occurs between 1.5 and 3 mm, and occurs later with shorter wavelength. A power law fit of the slopes of this second process yields a $\lambda^{-6.5}$ dependence, which is inconsistent with Rayleigh or Mie scattering. Following reshock, there is a sharp increase in the absorption across the entire spectrum. The rate of increase in the absorption displays weak wavelength dependence, and may indicate a second reaction. Eventually, the 400-500 nm (blue) channels saturate while the 500-650 nm (red) channels approach saturation; the experiment ends when the shock wave reaches the window/vacuum surface. Absorption changes following reshock are nearly linear with respect to distance until absorption approaches saturation, giving a sigmoidal appearance.

Increasing the shock pressure to 28.6 GPa (Figure 3b) leads to a steeper rise in absorption compared to 27 GPa. The approach to saturation is fastest in the 400 nm channel, requiring $\sim$ 2.5 mm of cyclohexane to be transited by the shock. The distinct separation of absorption at 400 nm is no longer apparent, and a smooth wavelength dependence is seen in the 400-600 nm region. The 600 nm and 650 nm channels remain similar to each other, as they did at 27 GPa. We note the presence of sharp rises in absorption upon breakout in the 450 and 500 nm channels, instead of the constant slopes seen in other channels. The change in slope observed following reshock is evident but less pronounced.

At 31.1 GPa, absorption increases again (Figure 3c). At 400 nm, the mass thickness that must be shocked to reach saturation is $\sim$ 0.5 mm, compared to over 5 mm at 27 GPa. The 600 nm and 650 nm channels are distinct from each other. The change in slope prior to

reshock observed at lower pressures is still faintly visible in the 650 nm channel at 31.1 GPa. (The apparent oscillations in the 650 nm channel are due to oscilloscope noise.) A change in slope upon reshock is observed only in the 600-650 nm channels; the other channels are saturated before reshock.

Further increasing the pressure to 33.1 GPa steepens absorption again for $\lambda < 550$ nm, and shows a smooth wavelength dependence in absorption (Figure 3d). In contrast, we note a curious change in the response at 600 and 650 nm. Instead of an increasing absorption, both channels show less absorption at this pressure. The 650 nm channel actually shows the emission of light. The apparent emission of light persists for ~ 3 mm (350 ns), followed by a sudden change to a linearly increasing absorption. This emission occurs on this channel alone. No change in slope is seen upon reshock, even at wavelengths where the signal is not saturated. This emission has two probable origins, luminescence of the reacting cyclohexane, or thermal emission.

Luminescence mechanisms under shock are difficult to address, so we have corrected for thermal emission on this shot, as shown in Figures 3d and 4e. In both of these cases, the uncorrected data are shown in black, with an appropriate fit to guide the eye, and the corrected data are shown in color. The cyclohexane is expected to be roughly 2500 K and the Al baseplate 2700 K at this pressure. It is also possible that the quartz window could be radiatively heated prior to shock arrival in the quartz itself. The linear increase in the emission with time suggests that it arises from the sample volume; were the source the Al baseplate, emission should only decrease as more cyclohexane is shocked and becomes absorbing, and as heat is transferred to the cyclohexane. Likewise, if the source is the quartz window, emission should only increase as more shocked cyclohexane can radiate; we should not see the decrease in emission seen at 3 mm. Thus in our corrections we assume that the thermal emission arises from cyclohexane with a color temperature of 2500 K. We have modeled the emission as linearly increasing with time (and therefore distance). This time-dependent increase in temperature was scaled according to expected emission for the central wavelength of the detector, and subtracted from the absorption signal. Absorption signals were then normalized to 0.95 at peak to have similar scaling to the uncorrected data. The thermal correction is most notable for the 650 nm channel; in the case of the 400 nm channel the original and corrected data lay atop each other, and the corrected data are not shown to improve clarity. In Figure 4, the thermally corrected data are only shown in 4e, for 650 nm.

As shown in Figure 3d, if this thermal emission model is correct, then cyclohexane absorbs relatively little in the red for the first ∼280 ns, at which point the absorption increases. This can be explained through several mechanisms, including nucleation of sufficiently sized scattering particles or chemical incubation times. With the thermal correction, there is still no change in absorption slope upon reshock, suggesting that scattering in the quartz window is not a major contributor; we would expect scattering from microcrystals to increase the apparent absorption rate.

An alternate way to examine the data is to consider the effect of increasing pressure at a fixed wavelength. Taking the 450 nm signal as an example (Figure 4b), we see that at the lowest pressure, there are at least two processes that affect absorption. As the pressure increases, the absorbance increases. At intermediate pressures, it appears that there are still two processes, but the absorption associated with the first process is much stronger, indicating a faster initial reaction rate (assuming it is the same set of reactions). At the highest pressures, only one process is apparent, leading to final highly absorbing product that is rapidly produced. It is unknown if the first set of reactions outcompetes the second, or if a new reaction combination is introduced. This change with pressure is seen at 400, 450, and 500 nm. In the red wavelengths, the changes are different. While generally the absorption increases with pressure, an exception occurs at 33.1 GPa. In this case, the absorbance decreases compared to the other pressures, and in the case of the 650 nm signal, we see overall emission at 33.1 GPa. This emission suggests a new process is occurring, for example, thermal emission from the cyclohexane, or a luminescence mechanism. After correcting for this emission a reduced absorption is still seen. This may indicate that the thermal correction is insufficient, or that the higher pressure impedes absorption at this wavelength (e.g., through greater fragmentation rates of species that absorb in the red). We note that the absorption rate (i.e., slope) at 650 nm at later times is similar regardless of pressure, but has different onset times. The absence of a change in slope upon reshock suggests that an increase in pressure does not affect the reaction or the quartz window at this pressure.

C. Absorption in benzene

Figure 5 shows the absorption in benzene shocked to 12 and 18 GPa. Benzene is typically thought to react around 13 GPa; the benzene Hugoniot used in this paper [1] lists the reacting region as 13.3 to 19.4 GPa. Figure 5 shows that absorption in benzene begins to change at pressures as low as 12 GPa; this is consistent with the results of Holmes,[23] which showed significant benzene absorption at 450 nm at 12.8 GPa. A clear incubation period lasting ∼70 ns is observed at 12 GPa, after which absorption saturates in a 150 ns period. In contrast, no incubation period is seen in the 18 GPa data; absorption rises immediately upon breakout and saturates within 15 ns. No comments can be made on the effect of reshock as absorption was fully saturated and no changes were seen.

V. DISCUSSION

Examination of the data shows that response in each cyclohexane channel is primarily described by linear segments, with the exception of a slow sub-linear change as saturation is approached. This suggests that reactions occur as the shock passes (see section IIIB), reaching a temporary equilibrium which lasts for at least 100 ns. Reactions occurring during this time within the compressed post-shock region are weak contributors to absorption/scattering. The observed immediate rise in scattering and emission, not accounted for by surface roughening, is consistent with this model of an initial fast reaction. We note that there is significant variation in the sharpness that depends on both wavelength and pressure. The pressure dependence of this variation is most noticeable in the 400 nm data (Fig. 4a), where a sharp rise in absorption occurs upon breakout, and is followed by a decreased absorption rate. This change in $B[t]$ occurs in the region closest to the Al baseplate; however, from these data it is not possible to determine the origin of this sharp rise, e.g., if the Al interface is increasing absorption in this band.

The slow change in absorption as saturation is approached (A > 90%) is consistent with a nonlinear response (as observed in high concentration solutions under ambient conditions) and indicates Beer's Law no longer applies. Slow changes in absorption at lower saturation levels indicate that another mechanism is at play. Such changes can be seen most clearly in the 600 and 650 nm data of Fig. 3c, after ∼3.5 nm transit, and the 550 nm data of Fig. 3d,

after ∼3 nm transit. A decrease in absorption rate is also evident at 27 GPa in Fig. 3a at $\lambda \geq 450$ nm, where it occurs after 1-2 mm transit (100-200 ns). This change occurs earlier at longer wavelengths. After this point, we observe that absorption at 27 GPa is wavelength dependent. In all cases, these decreases happen before reshock occurs while the pressure is constant. Because the shock front is steady, reactions at the shock front are unlikely to vary with time.

This change in absorption rate indicates that cyclohexane/shock product solution reacts following the initial temporary equilibrium. This would not be inconsistent with a two-wave model, shown in Fig. 6 and observed in many reactive systems. In this model, the shock front separates in the reacting sample, with the initial shock compressing the sample and likely creating radicals. As the sample reacts and changes, a second wave responsible for further reactions separates from the first. Such reactive samples often show an induction time; in this case, a 40 ns induction time may be seen in the 400 nm data on this shot (Fig. 3a, inset), though it is not evident on any other cyclohexane channel. We did not have velocity gauges embedded in the sample to measure the structures, so direct confirmation of a two-wave structure is not possible. An alternate model may suffice to describe the cyclohexane reactions.

The absorption decrease seen at 31 GPa is due to a different mechanism (that is, it is not an induction time). In this case, the decrease may be due to the consumption of absorbants in subsequent reactions; for example, if the absorbant were a relatively long carbon chain, fragmentation could lead to a decrease in absorbant concentration.

Most channels show an absorption slope change following reshock. This slope change indicates that there are reshock-induced reactions as the sample is compressed again. As discussed earlier, the formation of microcrystals in the quartz window may affect scattering and absorption. However, no absorption changes were seen at the highest pressure upon reshock, which suggests that the effect of such microcrystals is minimal and the observed effects at lower pressures are genuine. Reshocks do not impart the high heat of a first shock, so provide an opportunity to study reaction kinetics. (For example, a first shock state may have T= 2100K and pressure P, while the reshock state has T=2800K and pressure $1.8P$.)

This rise in absorption due to reshock occurs ∼50 ns after reshock from the window is expected to enter the cyclohexane at the three lowest pressures. There are several possible origins for this delay: a physical or chemical process occurring upon reshock; an incorrect

measurement of the cell window thickness; and an incorrect shock velocity for cyclohexane. An incorrect cell window thickness is unlikely to be the origin; this delay corresponds to a .44 mm error in measurement, and our machining tolerances are of .01 mm. Likewise, the shock velocity would need to be incorrect by ∼8%, or ∼0.7 km/s, which is roughly double the uncertainty in shock velocity. Therefore, we conclude that the most likely origin of this delay is a physical process or chemical reaction. We believe that scattering at the quartz window interface is unlikely to be the origin; approximately 350 μm of quartz would be shocked at this point, and if scattering arises from the quartz, theory suggests we should see it after a few microns of shocked quartz. As a result, we will analyze the observed changes upon reshock as though they are due to chemical reactions.

The long times between reshock and this absorption change indicates that the reaction kinetics are slower, an incubation period is needed, or that a multi-wave structure may evolve. We cannot distinguish between a reshock-induced reaction with an incubation time that does not require a multi-wave structure (occurring after point A in Fig. 6), and the interaction of a slower reaction wave front with either the compression reshock wave (point B, Fig.6) or the quartz interface (point C, Fig. 6).

We assume that the cyclohexane eventually experiences a single final reshock pressure and temperature, with one set of associated reactions at each pressure. Under this assumption, the decreasing absorption following reshock seen in the 650 and 600 nm channels indicates that the reshock reaction is slower and involves the consumption of absorbing products. This could be verified through reshock Hugoniot measurements and additional spectroscopic studies. Additionally, the cyclohexane Hugoniot at P $>$ 43 GPa has not been measured, which is the approximate reshock pressure. It is possible that cyclohexane undergoes a phase change at those pressures independently of the chemical changes we observe.

Mie scattering is a possible source of absorption and scattering in these experiments. However, Mie scattering is less probable than the formation of a conjugated polymer in this case. Typical recovered shock products contain ∼20-40 C atoms.[17] These products are far too small to create Mie scattering effects in the visible region; their absorption is determined by their electronic structure. Similarly, if Mie scattering were involved, the selective absorption seen at 27 GPa would suggest the unlikely result that 400 nm diameter particles can be produced, while 450 nm (and larger) particles cannot. We model Raleigh

and Mie scattering as power fits of the absorption strength to the wavelength:

$$A = c + d\lambda^n \tag{8}$$

where $n = -4$ indicates Rayleigh scattering and $-4 < n < 2$ is typical of Mie scattering. The absorption strength was plotted as a function of the central wavelength and power fits were applied. Results are shown in Table II. Values of n ranged from -2 to -6 and no trend in the values with increasing pressure was observed. Reshock models were limited by the high level of absorption prior to reshock, but all were inconsistent with Rayleigh or Mie scattering, with $n > 0$. For comparison, the wavelength dependence of absorption $A[\lambda]$ was also modeled as an exponential function; at all pressures, the exponential function was the better fit. The variation in scattering fits, combined with the distinct band at 400 nm, suggest absorption is due to chemical absorption bands common to hydrocarbons. Possible species include short (3-6 C) fragments and radicals whose HOMO-to-LUMO bands could be shifted into the visible from the UV by shock heating/compression or through the formation of longer conjugated chains.

A thermally induced shift of the HOMO-to-LUMO band in cyclohexane is unlikely. At ambient conditions, peak cyclohexane absorption occurs at 155-175 nm[26], indicative of a $\sim$7.5 eV HOMO-LUMO gap with a band edge at $\sim$7 eV. Absorption at 400 nm is equivalent to a $\sim$3.1 eV gap. For such a shift to occur only through thermal processes would imply that the cyclohexane temperature is roughly 40,000 K; such a temperature is unreasonable for a gas gun experiment, and significantly higher than the 2200-2500 K estimated for cyclohexane in these studies. No direct comparisons could be found in the literature for static pressure-induced visible absorption changes in either cyclohexane or benzene. Wen *et al.*[27] calculated benzene's band gap to shift from 4.5 eV at ambient, significantly lower than the $\sim$5.9 eV edge observed by Pickett *et al.*, [26] to $\sim$3.6 eV at 20 GPa and $\sim$2.5 eV at 40 GPa. These shifts would put benzene absorption in the visible region of the spectrum. This result is consistent with recovered samples of compressed benzene, which have a band edge located near 2.8 eV[2]. Assuming that static pressure-shifted cyclohexane absorption is also of 2 eV, one could expect the pressure-induced absorption edge in cyclohexane to be at $\sim$5 eV. After accounting for temperature-induced shifts, these results suggest a dynamically induced band gap closure of 1.7 eV, which would correlate to a band edge at $\sim$230 nm

at ambient. Molecular species with a single double bond, as might be expected from ring breaking, fragmentation, or dehydrogenation of the cyclohexane, typically have a band edge between 190 and 210 nm (6.2 and 5.9 eV) at ambient. While a band edge at 230 nm is somewhat higher energy than typically seen, it is more similar to a diene (e.g., 2-methyl-1,3-butadiene). A free radical structure is also possible, which could lead to a similarly scaled band shift.

TABLE II: Power law fits to absorption as a function of wavelength. * Uncorrected for thermal emission at 2500K. † Corrected for thermal emission at 2500 K.

Pressure (GPa)	Power fit	χ^2
33.1*	-.83 + 8.49e7 $\lambda^{-2.87}$	0.0103
33.1†	-.13 + 2.68e14 $\lambda^{-5.42}$	0.0156
31.1	-.043 + 2.4e10 $\lambda^{-4.0042}$	0.003
28.6	.034 + 22159 $\lambda^{-1.93}$	0.0127
27	.049 + 7.7e9 $\lambda^{-4.195}$	0.00037
27 process2	.053 -1.3e15 $\lambda^{-6.465}$	0.00010

For a fixed wavelength, increased pressure results in faster absorption, even when correcting for the faster shock front. Assuming that absorbance is proportional to absorbant concentration (Beer's law is true), this shows that the increased pressure and temperature of the harder shocks accelerates the reaction. These reactions are not observed in cold static compression experiments, nor are they seen in hot low pressure experiments. In the environment of a shock front, concentrations can be high and compression increases proximity. In combination with higher temperatures and additional unknown mechanisms, this may help to explain the uniqueness of these reactions.

One obvious explanation of the observed difference in the shock reactivities of benzene and cyclohexane is π bonding. The p-orbitals are involved in bonding to hydrogen atoms in cyclohexane. Polymerization in cyclohexane requires dehydrogenation first, and may be sterically hindered. In comparison, benzene does not need to be dehydrogenated if the projecting π bonds are involved in polymerization, and the conversion of a single C-C double bond to two C-C single bonds is energetically favored; the energy of a shock is ample (a 13 GPa shock imparts $\sim$500-600 kJ/mol to the compressed benzene and cyclohexane) to overcome an associated reaction barrier.

Finally, we note emission in the reddest bands at 33.1 GPa. There are at least two possible

explanations for this emission, which cannot be distinguished with these data. The first is the thermal emission of cyclohexane or the Al baseplate of the target. As the shock has not arrived at the quartz window, and such emission is seen immediately upon shock breakout into the cyclohexane, the quartz window can be excluded as the source of the emission. As the shock pressure increases, so does shock heating. Our detection system has a lower limit of 1500-2000 K, observed as increased signal in the reddest channels, with little change observed in the blue channels. A second explanation is the formation of an emitting dye molecule (luminescing polymer) in the shock. To test these hypotheses, spectrally resolved emission and absorption data must be collected at the pressure of interest.

The design of these experiments incorporates a reshock in the chemical sample from the quartz window. Such reshocks allow higher pressures to be probed, and can provide insight into the reaction kinetics. [28] One advantage of a reshock is that a similar pressure can be reached as in a single shock, but the temperature will be lower. At lower pressures, absorption upon reshock was observed to increase following a delay. At the highest pressure, absorption was seen to remain constant. Scattering in the quartz window would result in immediate increased absorption at all pressures, so we posit that these changes are indicative of reactions occurring upon reshock. However, the integrated nature of these experiments makes it difficult to extract temperature and pressure effects on kinetic rates upon reshock, as it must be measured against the pre-existing absorption levels, unknown pressure-induced band shifts, the unknown window effects, and the unknown reshock Hugoniot at these pressures. A modified target design could eliminate many of these problems (for example, by using LiF and improving spectral resolution), allowing future reshock measurements to be made.

VI. CONCLUSIONS

Cyclohexane is observed to react under shock compression at 27 GPa, with shock driven reactions overdriven by 33.1 GPa. This shows that the very small change in the cyclohexane Hugoniot observed at 22-32 GPa is due to shock driven reactions, analogous to the changes seen in the benzene Hugoniot at 10-13 GPa. The observation of reactions at 27 GPa, the lowest pressure in this study, constrains the onset of shock reactions in cyclohexane to between 18 and 27 GPa. Absorption changes were seen upon shock breakout, with no clear

incubation time in cyclohexane that would indicate a multi-wave structure. The presence of a multi-wave structure could not be directly determined with this experimental design. These were followed by constant absorption coefficients with time, indicating that these reactions occur within the shock front and are followed by a metastable non-reacting state until reshock. In contrast, benzene was shown to have an incubation time of ∼70 ns at 12 GPa prior to reaction. Following incubation, benzene quickly saturated.

These results are significant because they shed light on the reaction mechanisms of hydrocarbons at extreme pressures and temperatures. The shift in absorption bands in cyclohexane cannot be explained through a thermal mechanism. However, the formation of a π-bonded system of 2-4 C length would be consistent with the observed shifts. As the pressure is increased from 27 GPa, the absorption evolves from a slow linear increase to a rapid increase and eventual saturation. With increasing pressure, this behavior first observed in the shorter wavelengths happens at longer and longer wavelengths, indicating a smooth shift in absorption band edge. This suggests that the much lower reaction barrier of shocked benzene can be explained through the possibility of π bonds reacting in compression, while cyclohexane must first be dehydrogenated. Possible distinction of this reaction could be conveyed in measurements of the reshock Hugoniot, which would move through a different material.

VII. FUTURE WORK

These data indicate that a reaction occurs in cyclohexane within or near the shock front, with a possible second reaction upon reshock. The identification of the reaction conditions for cyclohexane means that it may serve as a model system for studying saturated hydrocarbon reactions *in situ*, which is important for understanding plastics and materials under extreme conditions. The constant absorption rates over long times indicate that cyclohexane would be a candidate for identifying mechanisms of shock reactions, which remain unknown. Some speculation about the mechanism is helpful in framing the direction of future work. The distinct absorption at 400 nm and 27 GPa rules out the formation of large 400+ nm particles that would cause Mie scattering. The lack of absorption at longer wavelengths at 27 GPa suggests that the 400 nm band is the red end of a broader absorption band with a peak in the UV region. It is well known that absorption bands due to HOMO-to-LUMO transitions

depend on conjugated chain length, with longer chains having redder absorption peaks; this is also true for conjugated radical species.[29] The observed absorption is consistent with that of short conjugated alkenes. The decreased selectivity in absorption observed at higher pressures is consistent with absorption band broadening due to either increased conjugated chain lengths or chemical and pressure induced changes in the electronic structure. The decreased absorption seen in the reddest wavelengths at higher pressures would also be consistent with this model; as chain length increases, less energy is required to break it, so red absorption observed with increased chain length would decrease. This decreased absorption could also be the result of competing reactions, e.g., polymerization and depolymerization. Increased spectral resolution could determine the degree of absorption broadening with pressure and would provide basic answers about chain length and electronic structure.

The delayed effect of reshock on absorption suggests that the observed change in absorption is due to a chemical reaction, and not to scattering in the shocked window. Future experiments should measure this explicitly to rule out window effects. Reactions upon reshock would be consistent with a phase change, reactions within the front (possibly in a two-wave structure), or decomposition. Measurement of the reshock Hugoniot and *in situ* particle velocities could resolve questions about reshock reactions. Increased absorption at long time could be due to cross-linking, consistent with the polymerization observed by Aoki *et al.* in compressed acetylene.[30] It is unlikely to be due to further fragmentation, as that would lead to decreased absorption. Raman spectroscopy would be best suited to monitor bands in possible intermediate products, such as the appearance of conjugation, and cyclohexane fragmentation.

VIII. ACKNOWLEDGMENTS

This work was performed under the auspices of the U.S. Department of Energy by Lawrence Livermore National Laboratory under Contract No. DE-AC52-07NA27344. Our thanks to Bob Nafzinger, Elida White, and David Layne for their technical support.

---

[1] R. D. Dick, J. Chem. Phys. **71**, 3203 (1979).

[2] P. Pruzan, J. C. Chervin, M. M. Thiery, J.P. Itie, J. M. Besson, J. P. Forgerit, and M. Revault, J. Chem. Phys. **92**, 6910 (1990).

[3] L. Ciabini, M. Santoro, R. Bini, and V. Schettino, J. Chem. Phys. **116**, 2928 (2002), and references therein.

[4] V. G. Baonza, Chem. Phys. Lett. **398**, 175 (2004).

[5] K. Shigematsu, H. Hondo, T. Kumagai, and Y. Takahashi, Cryst. Growth Des. **9**, 4674 (2009).

[6] J. Crain, W.C.K. Poon, A. Cairnssmith, and P.D. Hatton, J. Phys. Chem., **96**, 8168 (1992).

[7] J. Haines and D.F.R. Gilson, J. Phys. Chem., **93**, 7920 (1989).

[8] M. Pravica, Y. R. Shen, Z. Quine, E. Romano, and D. Hartnett, J. Chem. Phys. **111**, 4103 (2007).

[9] M. Pravica, Y. Shen, and M. F. Nicol, Appl. Phys. Lett. **84**, 5452 (2004).

[10] A. Matsuda, K.G. Nakamura, and K. Kondo, Phys. Rev. B, **65**, 174116 (2002).

[11] S. Oguchi, A. Matsuda, K. Kondo, and K. G. Nakamura, Jpn. J. Appl. Phys. Part 1 - Regul. Pap. Brief Commun. Rev. Pap. **45**, 5817 (2006).

[12] U. Steil, M. Braun-Unkhoff, C. Naumann, and P. Frank, Proceedings of the European Combustion Meeting 2005, Louvain-la-Neuve, Belgium, 2005.

[13] I. M. Voskoboinikov, Chem. Phys. Rep. **16**, 507 (1997).

[14] C. A. Bolme, S.D. McGrane, D.S. Moore, V.H. Whitley, and D.J. Funk, Appl. Phys. Lett. **93**, 191903 (2008).

[15] M.F. Gogulya and I.M. Voskoboinikov, Combust. Explos., **37**, 464 (2001).

[16] N.C. Dang, C.A. Bolme, D.S. Moore, S.D. McGrane,J. Phys. Chem. A, **116** 10301-10309 (2012).

[17] L. V. Barabe, A. N. Dremin, S. V. Pershin and V. V. Yakovlev, Fizika Goreniya i Vzryva **5**, 528 (1969).

[18] S.A. Sheffield, D.M. Dattelbaum, and D.B. Stahl, Shock Compression of Condensed Matter - 2009, Pts 1 and 2, Nashville, Tennessee, 2009, edited by M. L. Elert, W. T. Buttler, M. D. Furnish, W. W. Anderson and W. G. Proud (AIP, Melville, NY, 2009), Vol. 1195, p. 145.

[19] R.W. Woolfolk, M. Cowperthwaite, and R. Shaw, Thermochimica Acta **5**, 409 (1973).

[20] Y.B. Zel'dovich and Y.P. Raizer, *Physics of Shock Waves and High-Temperature Hydrodynamic Phenomena*. (Dover Publications, Inc., Mineola, NY, 2002).

[21] A.C. Mitchell and W.J. Nellis, J. Appl. Phys., **52** 3363 (1981).

[22] S.B. Kormer, Soviet Physics Uspekhi-Ussr, **11** 229 (1968).

[23] N. C. Holmes, Rev. Sci. Instrum. **64**, 357 (1993).

[24] S.-N. Luo, T. J. Ahrens, and P. D. Asimow, J. Geophys. Res.**108(B9), 2421 (2003).**

[25] There is one other condition where dB/dt would zero, if ϵ[t] = 1/C[t]. We neglect this unlikely scenario.

[26] L.W. Pickett, M. Muntz, and E.M. McPherson, J. Am. Chem. Soc., 73,4862-4865 (1951).

[27] X.-D. Wen, R. Hoffmann, and N. W. Ashcroft, J. Am. Chem. Soc., 133,9023-9035 (2011).

[28] S.A. Sheffield, J. Chem. Phys.,81,3048-3063 (1984).

[29] S. Tagawa,, N. Hayashi, Y. Yoshida, M. Washio, and Y. Tabata, Radiation Phys. and Chem. 34, 503 (1989).

[30] K. Aoki, Y. Kakudate, M. Yoshida, S. Usuba, K. Tanaka, and S. Fujiwara, Sol. St. Comm. 64, 1329 (1987).

IX. FIGURES

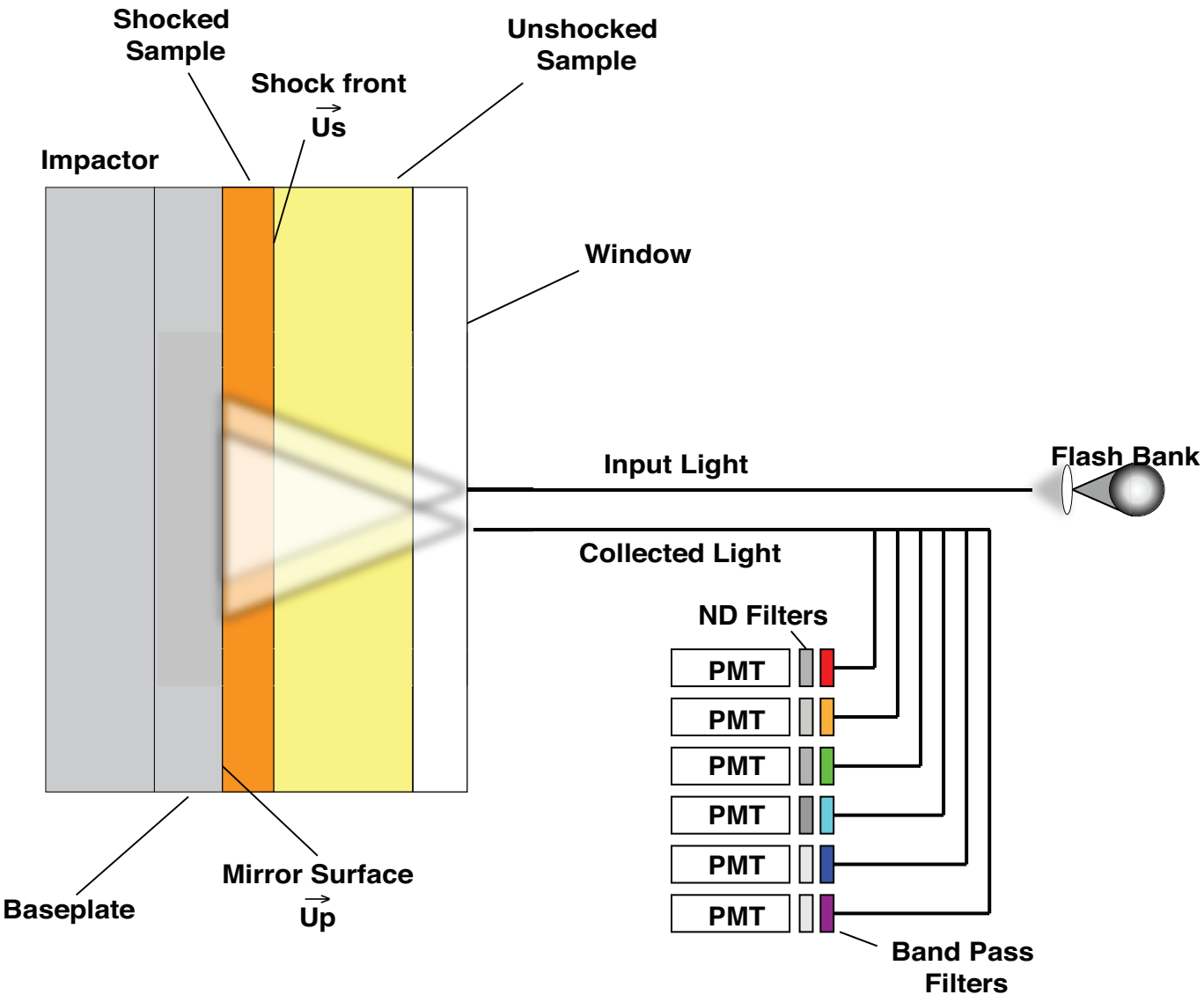

FIG. 1: Experimental set up for the shock double pass absorption experiment (not to scale). A central fiber illuminates the target using broadband light from a flash bank. Six adjacent fibers, shown here as a single fiber for simplicity, collect the reflected light and relay it to photomultiplier tubes (PMT) for detection. Each collection fiber had distinct band pass filters with appropriate neutral density (ND) filters to measure the spectral response in absorption. In this figure, the sample is shown as it would appear partway into the experiment. The shock launched by the impact of impactor into baseplate has fully transited the baseplate, and has entered the sample. The mirror surface of the baseplate and the region of shocked sample has a velocity of U_p; the unshocked region has a velocity of zero. The width of the shocked region changes as $(U_s - U_p)$t. The changing optical geometry caused by the motion of the mirror surface and the altered refractive index and width of the shocked region has been accounted for in the data shown in Figs. 3-4.

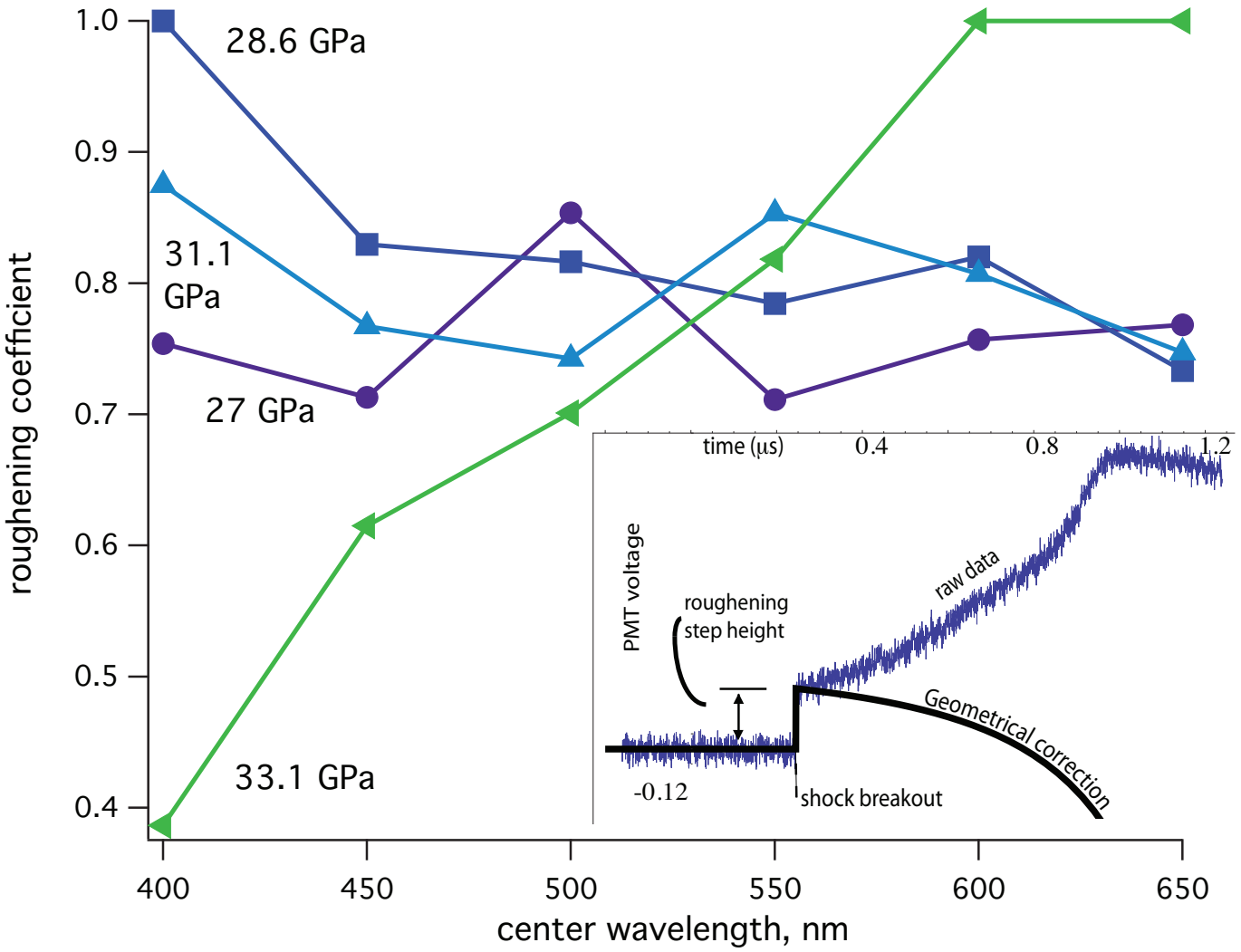

FIG. 2: Roughening factors used to correct raw data for each wavelength and pressure. Roughening is not strongly wavelength dependent at the lower pressures, but at 33.1 GPa is strongly dependent, suggesting all reactions are overdriven, leading to an extremely rapid change in the scattering centers. INSET: An example of raw data (blue, 28.6 GPa at 450 nm) and corrections (black). Prior to shock breakout, the negatively biased PMT has a steady voltage due to constant reflected light; upon breakout, surface roughening and other effects lead to a sharp loss in transmission and a resulting increase in PMT voltage ("step height"). The magnitude of this increase provides a rough estimate of roughening/scattering at the surface. The expected signal due to surface motion toward the collecting fibers, changes in refractive index in the shocked liquid, and total changes in path length are calculated and shown as the "geometrical correction." Note that as the sample moves toward the collecting fibers, the expected signal should increase, which is detected as a more negative PMT voltage. The difference in the geometrical correction and the raw data is the signal change due to absorption changes in the shocked sample, and is the corrected data. The result of the difference for this data set are shown in Fig. 3b as the 450 nm channel. All corrected data shown in subsequent plots are calculated this way.

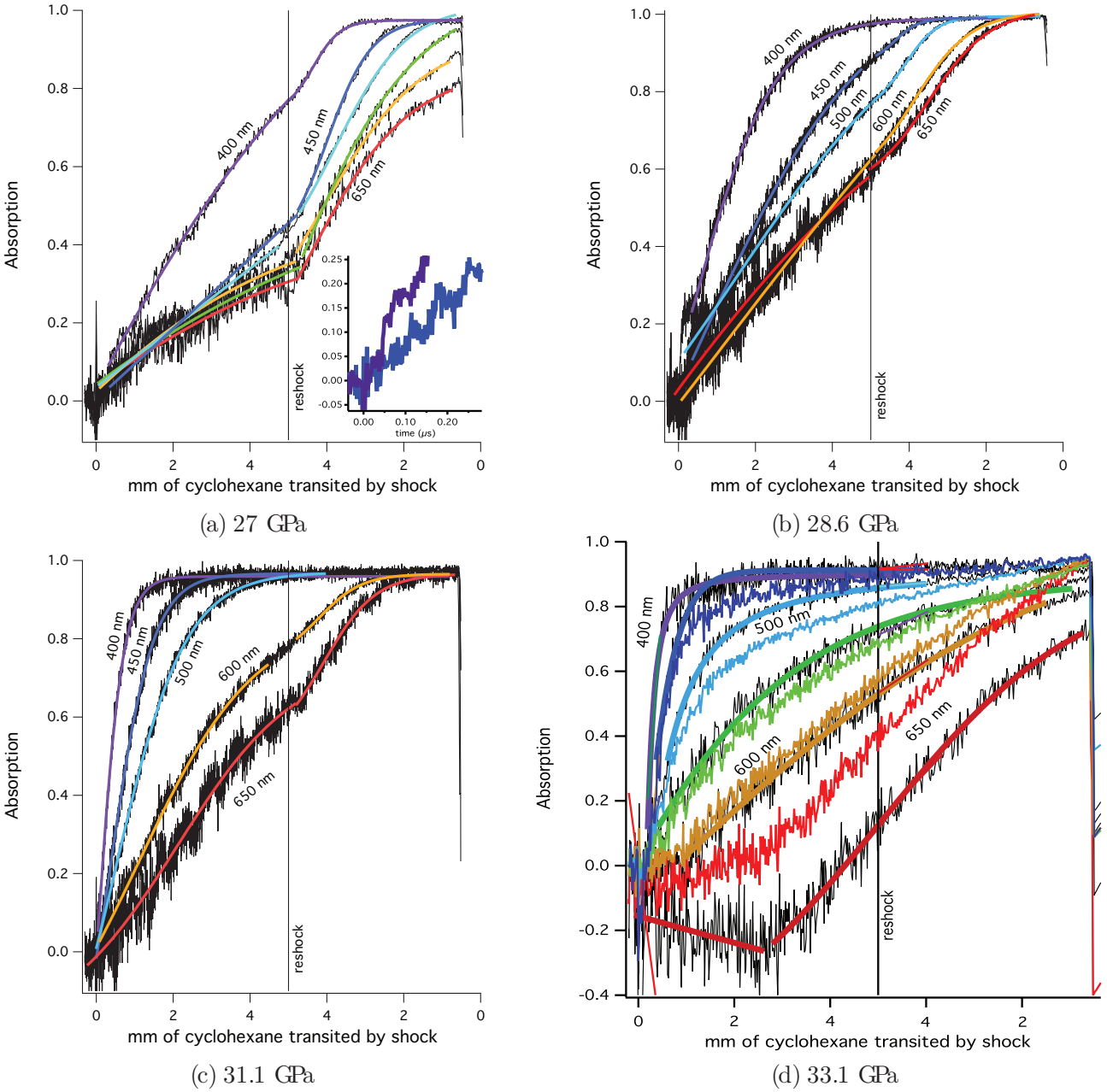

(a) 27 GPa

(b) 28.6 GPa

(c) 31.1 GPa

(d) 33.1 GPa

FIG. 3: Wavelength dependence of absorption at each pressure: a)27±0.6 GPa, b) 28.6±0.6 GPa, c) 31.1±0.6 GPa, and d) 33.1±0.7 GPa. Thermal corrections applied at 33.1 GPa are shown in color. Center wavelengths shown at each pressure are 400, 450, 500, 550, 600, and 650 nm. 550 nm data are collected on two shots, a) and d). The larger noise levels on the 650 nm data are due to noise problems with that oscilloscope channel, and enhanced relative to late times by the geometric correction. Reshock occurs when the shock hit the window after transiting 5 mm cyclohexane, where it is reflected. To indicate this reflection, the x-axis shows the Lagrangian position of the shock (or reshock) front in the cyclohexane, based on the calculated (re)shock speed. Reading from the left, 0 to 5mm are transited by the shock; at 5 mm the reshock reflects and returns toward the Al baseplate located at 0 mm. Note that in all cases, the experiment ends, due to collecting fibers being destroyed, before the reshock arrives at the Al interface. Inset of Fig. 3a shows the absorption at breakout, including the ∼40 ns incubation time at 400 nm.

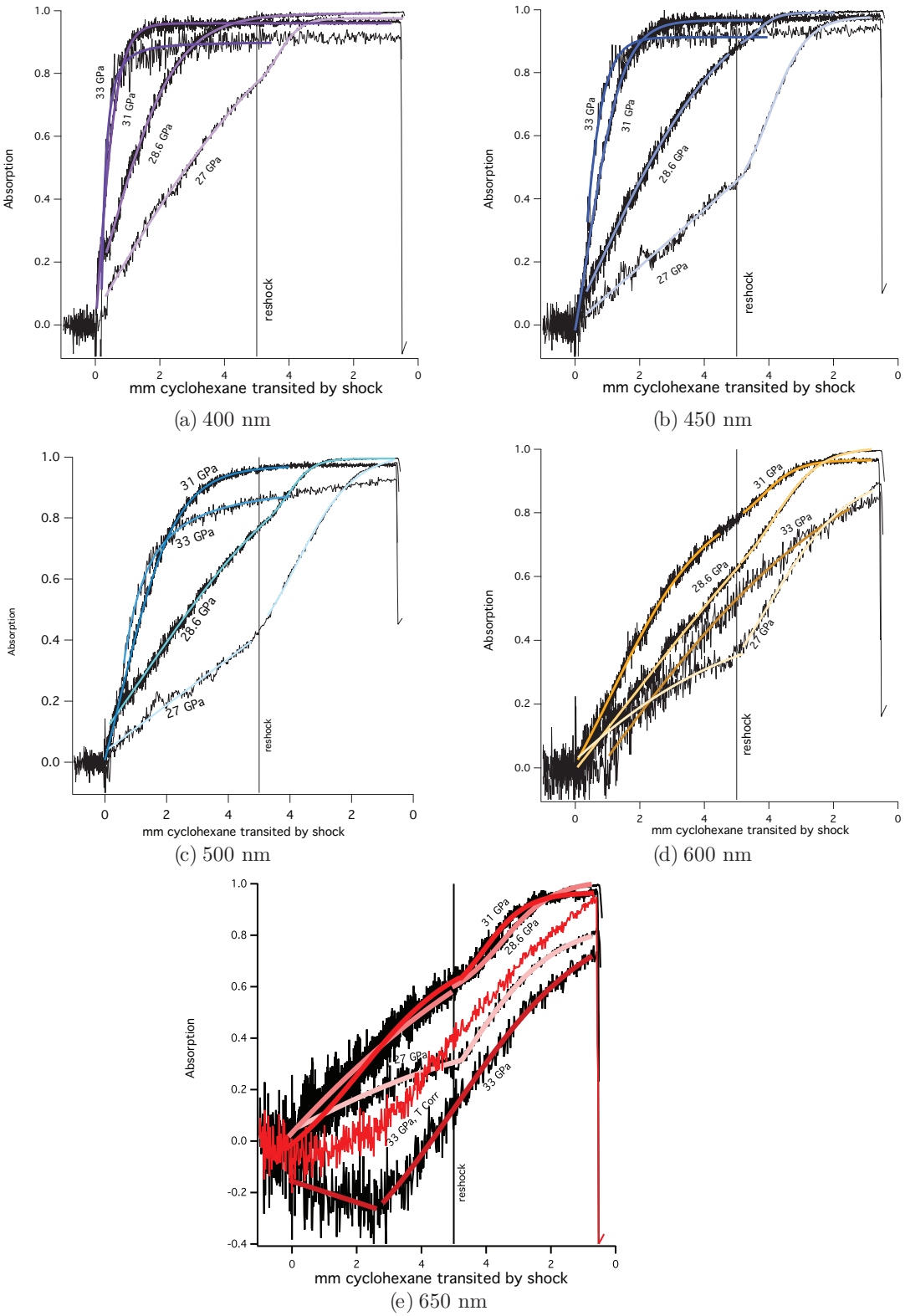

(a) 400 nm

(b) 450 nm

(c) 500 nm

(d) 600 nm

(e) 650 nm

FIG. 4: Pressure dependence of absorption at each wavelength. Center wavelengths shown are a) 400 nm b) 450 nm c) 500 nm d) 600 nm and e) 650 nm. The larger noise levels on the 650 nm data are due to the aforementioned noise problems with that oscilloscope channel. Fits are shown to guide the eye. The thermally corrected signal at 650 nm is shown in red in Fig. 4e.

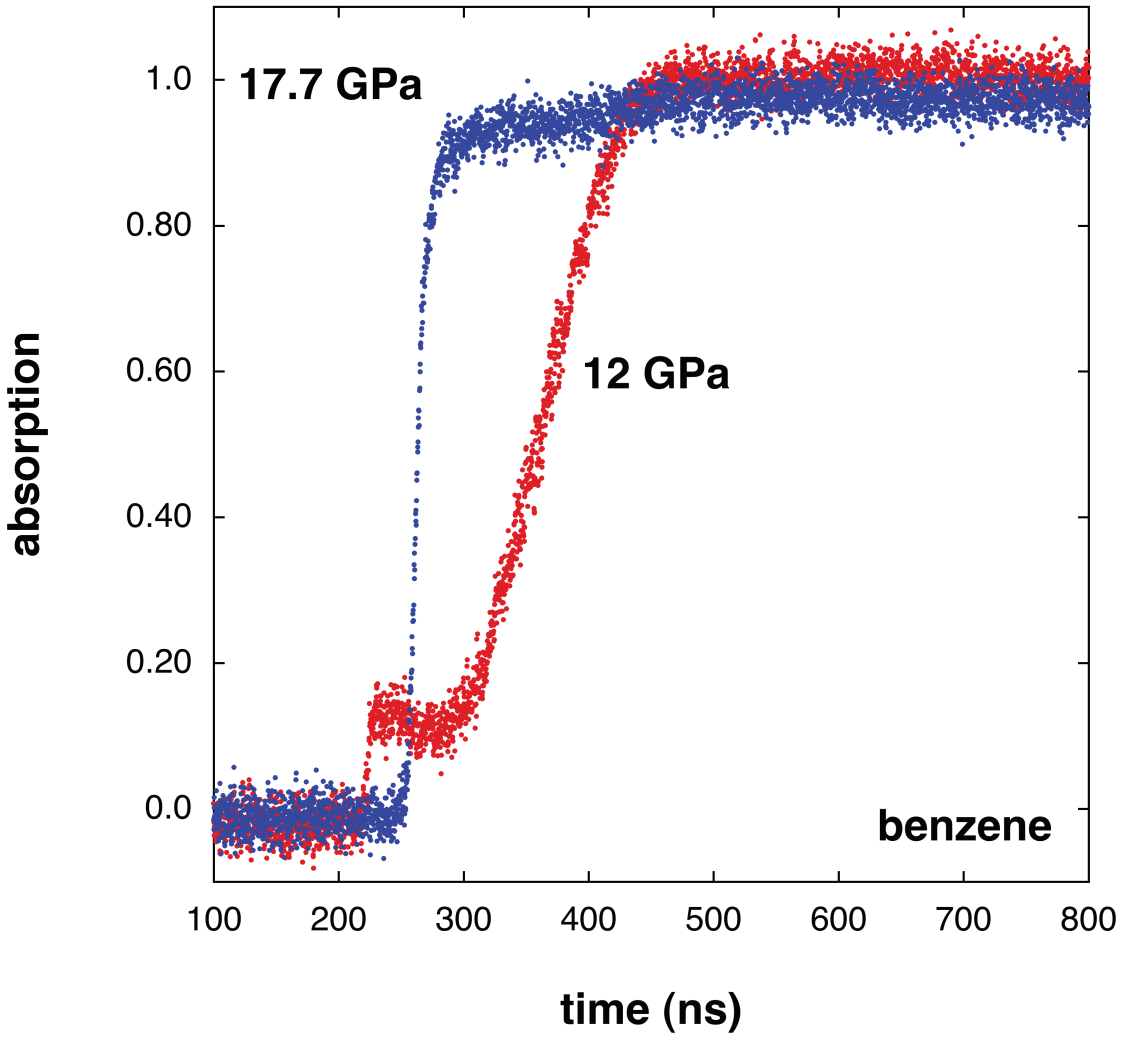

FIG. 5: Absorption of benzene at 532 nm shocked to 12 and 17.7 GPa. Breakouts are offset in time for clarity. Note the pronounced incubation time at 12 GPa which disappears at 17.7 GPa.

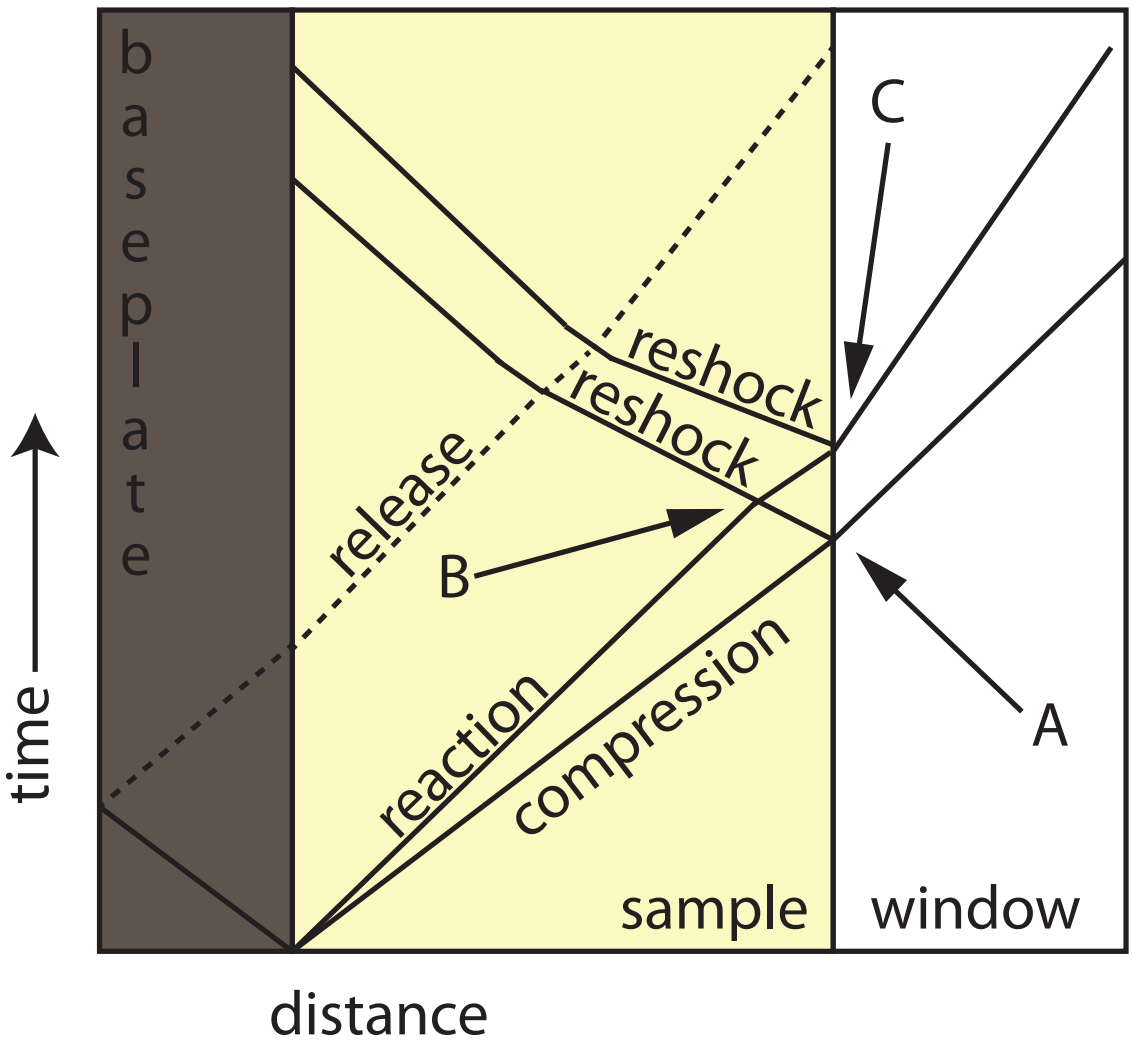

FIG. 6: A distance-time diagram of possible wave interactions in a reacting sample. Each angled line segment in the diagram shows the wave's characteristic, or the path of information propagation. Upon impact, shock waves are launched into the sample and into the baseplate/flyer material (here noted as "baseplate"). In the simplest multi-wave model, the shock front in the sample separates into a compression wave, which compresses the sample without reacting it, and a reaction wave, which reacts the now compressed sample. (More complex models exist, e.g., with multiple reaction waves.) Upon arrival of the shock at the baseplate/flyer edge, the pressure drops, and a release wave propagates forward. Upon arrival of the shock fronts at the window interface, the shock is reflected back into the sample; these reflections interact with other shock fronts, e.g., the reflection of the first shock with the slower-moving reactive front, and the release waves, to create multiple pressure and temperature zones in the sample.